

Experimental Evidence for Two-Step Nucleation in Colloidal Crystallization

J. R. Savage* and A. D. Dinsmore

Department of Physics, University of Massachusetts, Amherst, Massachusetts 01003, USA

(Received 30 October 2008; published 15 May 2009)

We investigated the freezing of colloidal spheres in two dimensions with single-particle resolution. Using micron-size, charge-stabilized polystyrene spheres with a temperature-dependent depletion attraction induced by surfactant micelles, we supercooled an initially amorphous (gaslike) system. Particle motions were monitored as crystallization proceeded. At low concentrations, freezing occurred in a single step in a manner consistent with classical nucleation theory. In other samples two-step nucleation was found, in which amorphous clusters grew to ≈ 30 particles, then rapidly crystallized. Measured free energies show the role of metastable gas-liquid coexistence, which also enhanced the rate of nucleation following deeper quenches.

DOI: [10.1103/PhysRevLett.102.198302](https://doi.org/10.1103/PhysRevLett.102.198302)

PACS numbers: 82.70.Dd, 64.60.My, 64.70.pv, 81.10.-h

The formation of crystals by atoms, molecules or particles following a temperature quench is important in many natural situations and applications but still the subject of active investigations [1–3]. The classical nucleation theory, often used to describe the process, assumes that small clusters form with the same structure as the new phase but that the interfacial energy leads to a rate-limiting free-energy barrier and a minimum size for stable clusters [1–4]. An alternative approach, supported by growing experimental evidence [5,6], predicts instead that phase separation can occur by the sample’s passing through multiple states in order of decreasing free energy [2,5,7,8]. Systems with short-range centro-symmetric attraction, such as colloids and globular proteins in solution, provide a practical and relevant example of the distinction between these two mechanisms. Computer simulations [3,9–11] and theoretical models [12–16] predict that the starting fluid might not form crystals directly, but instead form a metastable liquid phase consisting of a higher-than-average concentration, then crystallize. This two-step nucleation pathway is predicted to reduce the free-energy barrier and enhance the crystallization rate. Experiments with protein solutions show that crystallites nucleate within metastable liquid-phase droplets [17] or evolve from metastable clusters [18], and that the nucleation rate density is maximum near the metastable gas-liquid (*g-l*) boundary [19]. These experiments suggest that two-step nucleation occurs over a broader region of phase space than initially predicted [9,12], consistent with more recent theory [16]. These experiments did not, however, probe the evolving structure of individual particles and clusters. The use of colloidal particles, on the other hand, allows experimental studies of phase transitions with single-particle resolution and with tunable interparticle interactions. This approach has proven useful to study melting [20–25], and freezing of nearly-hard spheres [26].

Studies of colloidal particles in 2D that attract one another by electric-field-induced flow revealed two-step

nucleation of crystallites within dense liquid droplets. The interaction, however, was of long range and possibly dependent on cluster size, and the fluid flow might alter the dynamics [27]. Earlier studies of freezing in 2D colloids with short-range attraction reported a scaling of the cluster-size distribution and a two-step nucleation process, with amorphous clusters appearing first and crystalline clusters later [21]. In the present work, we clarify the freezing dynamics with very short-ranged pair interactions by monitoring the size and evolving symmetry of individual clusters throughout freezing. We measured the free-energy landscape and show that the two-step mechanism (growing, then ordering) reduces effective line tension and lowers the free-energy barrier when the area fraction η is not small. Moreover, quenching to within the metastable *g-l* coexistence region greatly enhances the nucleation rate.

We used video microscopy to track charge-stabilized polystyrene spheres dispersed in Millipore-filtered water. The average sphere radius, R , was $0.7 \mu\text{m}$ with a polydispersity of 3.5%. Nonionic surfactant, hexaethylene glycol monodocecyl ether (C_{12}E_6), was added at sufficient concentration ($\sim 4.4 \times 10^{-2} \text{M}$) to form micelles of radius $R_m = 9\text{--}17 \text{nm}$. The micelles induce a depletion attraction between the spheres, the strength of which is $\Delta F_d/(k_B T) \approx -2\pi R R_m(T)^2 c_m(T)$, where $\Delta F_d/(k_B T)$ is the change in Helmholtz free energy and $c_m(T)$ is the concentration of micelles. For nonionic surfactants such as C_{12}E_6 , the critical micelle concentration decreases [28] and R_m increases [29] with T ; increasing T leads to stronger depletion and hence “supercooling” and freezing [24].

Our procedure was first to form a 2D weakly-interacting gas of spheres on the coverslip, then supercool the gas to induce freezing. Particles were bound to the flat coverslip (but were still mobile) by a depletion attraction whose magnitude is approximately $2\Delta F_d$ [24]. After a few minutes, samples typically contained crystallites with triangular symmetry coexisting with a dilute gas of spheres.

Images were acquired at 30 s^{-1} using an inverted optical microscope with a $63 \times$ oil objective, CCD camera, and S-VHS recorder. The microscope was placed in an insulating box on a mechanically isolated table. Samples were heated with an objective heater (Zeiss Tempcontrol 37). Unless otherwise indicated, final T was between 26 and 29°C . Data were acquired after enough time had passed for T to stabilize; temperature fluctuations afterwards were $\pm 0.1^\circ\text{C}$. Sphere positions were measured to within 45 nm using routines [30] written in IDL. A cluster is defined as the set of particles that were contiguously bonded, i.e., whose center-to-center distances $< 1.529 \mu\text{m}$ [24]. This cutoff length is slightly larger than $2(R + R_m)$, the range of the depletion attraction. The number of particles in a cluster is defined as N .

In supercooled samples, a large number of clusters appeared with a wide range of sizes. Representative images are provided in the supplemental information [31]. In most samples, these clusters were metastable and ultimately broke up. They had liquidlike mobility and were also amorphous, as shown by the average sixfold bond-orientational order parameter. Following convention, we define $\langle |\psi_6|^2 \rangle \equiv \langle |(1/Z_j) \sum_k \exp[6i\theta_{jk}]|^2 \rangle$ where Z_j is the number of bonds with the j th particle, the sum is over all bonded neighbors k , and θ_{jk} is the angle between the j - k bond and the x axis. The average $\langle |\psi_6|^2 \rangle$ is computed for all particles j within a cluster. Particles with $Z = 1$ have $\psi_6 \equiv 0$. Clusters having a perfect triangular lattice would have $|\psi_6|^2 = 1.0$ even if $Z < 6$, whereas disordered clusters have $|\psi_6|^2$ approaching 0. $\langle |\psi_6|^2 \rangle_{\text{av}}(N)$ is defined as

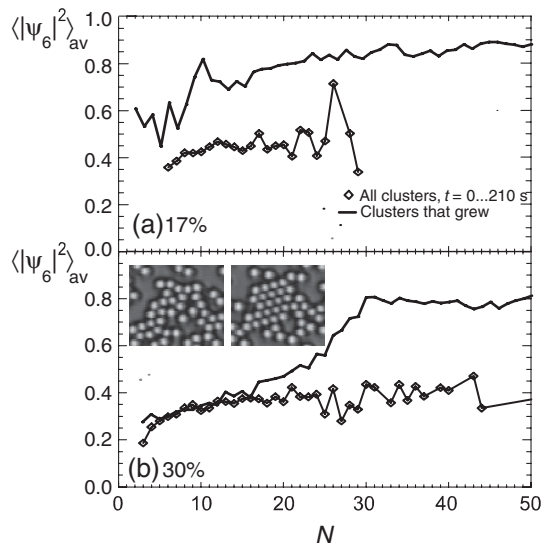


FIG. 1. Measured bond-orientational order parameter of clusters, $\langle |\psi_6|^2 \rangle_{\text{av}}$ vs. cluster size N . The samples have (a) area fraction $\eta = 17\%$ and $T = 28^\circ\text{C}$, and (b) $\eta = 30\%$ and $T = 29^\circ\text{C}$. The diamonds show results for all clusters in the samples. The solid curves show the data only for clusters that eventually form large stable crystallites [7 and 4 clusters, respectively, in (a, b)]. The two inset images in (b) show a region at two times separated by 90 s.

$\langle |\psi_6|^2 \rangle_{\text{av}}$ averaged over all clusters of size N . Figure 1 shows data for two samples at times $t < 210 \text{ s}$, prior to the formation of crystallites (\blacklozenge). The samples have colloid area fractions, $\eta = 17\%$ and 30% . These clusters appeared amorphous to the eye and, correspondingly had relatively low $\langle |\psi_6|^2 \rangle_{\text{av}} \approx 0.4$.

Clusters that ultimately became large crystallites followed a different path, shown by the solid curves in Fig. 1. In the 17% sample, these clusters had $\langle |\psi_6|^2 \rangle_{\text{av}} > 0.7$, even when $N < 10$. Hence they were quite distinct from the amorphous clusters and already had the order characteristic of the late-stage crystallites. This pathway is consistent with the classical nucleation model.

In the 30% sample, however, crystallizing clusters passed through two distinct stages during nucleation. In the first stage ($N < 20$), the clusters were amorphous and indistinguishable from the background. At intermediate sizes, there was a clear change in the slope and clusters became ordered when $N > 30$ ($\langle |\psi_6|^2 \rangle_{\text{av}} \sim 0.8$). This sudden ordering occurred throughout the clusters, even for particles with $Z < 6$ [31]. This two-step pathway differs strikingly from the classical nucleation model. The images in the inset of Fig. 1(b) show an example of the rapid evolution of a cluster from amorphous to crystalline.

Behavior intermediate between classical-nucleation-like and two-step was exhibited by a range of samples. Figure 2 shows $\langle |\psi_6|^2 \rangle_{\text{av}}$ vs. N for all clusters that grew to stable size, in samples with a range of η from 17%–34%. These samples also contained many “background” amorphous clusters like those of Fig. 1, \blacklozenge . Individual clusters appeared and vanished but the average size was approximately stationary during the first ~ 3 min, prior to appearance of the large stable crystallites [31].

Two other samples, with $\eta = 28.5\%$ and 34% and deeper quench ($T = 35$ and 30°C), showed markedly different dynamics. (Recall that freezing occurred with increasing T because of the micelles). As in other samples, amorphous clusters ($\langle |\psi_6|^2 \rangle_{\text{av}} \approx 0.5$) appeared spontaneously. In these cases, however, the average cluster size $\langle N \rangle$ increased with time, from 15 to 70 ($\eta = 28.5\%$) and from 15 to 35 (34%) over 400 s [31]. Because of this rapid growth of amorphous (l) clusters, we concluded that these

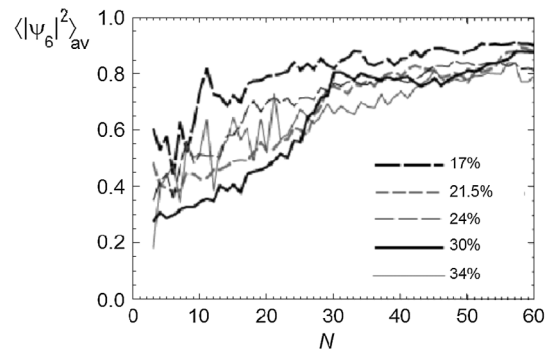


FIG. 2. Measured order parameter, $\langle |\psi_6|^2 \rangle_{\text{av}}$, for clusters that grow in samples with a range of area fractions, η .

samples lay within the metastable g - l coexistence region. We return to this point below in the context of measured free energy.

The nucleation rate density varied greatly among these samples. In the 28.5%/35 °C sample, 60 stable crystallites appeared within the first 3 min in an area of $1.37 \times 10^4 \mu\text{m}^2$. The 34%/30 °C sample contained 25 crystallites over the same time and area. By contrast, the samples with stationary $\langle N \rangle$ contained at most 4 stable crystallites after 3 min, and some samples showed no stable crystallites for more than 5 min. Hence the nucleation rate was enhanced by 1–2 orders of magnitude by crossing the metastable g - l binodal. This result is consistent with simulations [9,10] and density-functional theory [12,16], which predict large enhancement of the crystallization rate near the metastable g - l critical point. In our experiments, however, the two-step nucleation was also observed in samples (e.g., 30%) that lay outside the metastable g - l coexistence region.

This system has a very short-range attraction relative to the sphere size; i.e., $R_m/R = (1.3\text{--}2.4) \times 10^{-2}$. In such systems g - l coexistence is not found in equilibrium. Instead liquid clusters eventually crystallize or evaporate (see [2,32–37] and references in [9]). Microscopically, the liquid’s metastability may be explained by the loss of many (short-range) bonds when a crystalline cluster lowers its density and attains liquidlike mobility [35]. For small clusters, however, the interfacial tension Γ plays a key role. The gas-crystal interface should have large Γ owing to the large density mismatch [13,27,38]. The g - l interface, on the other hand, would have lower density mismatch and hence smaller Γ [13,27,38]. When the pair interaction is weak (as in a shallow quench), therefore, the lower Γ of the liquid can compensate for its less favorable bulk free energy and favor two-step nucleation.

For a direct look at the energetics, we obtained the chemical potential μ and line tension Γ of the transient liquid clusters from the number density of cluster sizes, n_N . Before stable crystallites appeared, clusters fluctuated in size but n_N did not change significantly over time. In this regime, n_N should follow the Boltzmann distribution; the free energy of clusters relative to monomers is therefore $-k_B T \ln(n_N/n_1)$. We fit the measured $-\ln(n_N/n_1)$ to the function $(\Delta\mu)N + (\eta_c^{1/2} \pi \Gamma)N^{1/2}$. Here, $\Delta\mu$ is the chemical potential of the amorphous clusters minus that of the gas. The second term represents the interfacial energy; Γ is the line tension in units of $k_B T$ per sphere diameter and η_c is the area fraction of the cluster. For numerical simplicity, we assume clusters were circular and set $\eta_c = (3/\pi)^2 = 0.91$ [31]. For the 17% and 30% samples, we look at data for $0 < t < 100$ s, before stable crystalline clusters appeared. We obtained good fits to the data [31]. We found $\Delta\mu$ to be small but positive [$0.10(4)k_B T$ ($\eta = 17\%$) and $0.04(2)k_B T$ ($\eta = 30\%$)], confirming that these samples lay outside the metastable g - l coexistence region. We found $\Gamma = 0.41(5)$ ($\eta = 17\%$) and $0.47(3)$ (30%). A few minutes later, stable crystallites appeared in these samples and $\Delta\mu$

became slightly negative as expected, since large crystalline clusters were stable. At the same time, the best-fit Γ increased to $0.68(3)$ in both samples. Hence the crystallites had larger interfacial energy than liquid clusters of the same N . The 30% sample had rather small $\Delta\mu$, so that the lower Γ of liquid clusters made them favorable compared to crystals and the two-step pathway was followed. Conversely, the 17% sample had larger $\Delta\mu$ so that fluid clusters cost too much energy to play a significant role in crystallization.

The 28.5% and 34% samples both had $\Gamma = 0.48$ and $\Delta\mu = -0.06(1)k_B T$ for $t < 100$ s. The negative $\Delta\mu$ is consistent with their lying within the metastable g - l region. During these early times, these samples appeared to undergo classical nucleation of the liquid clusters, followed by crystallization.

The free-energy landscapes of growing clusters show how their growth trajectories optimized both size and crystalline order. We introduce N_c as the number of crystalline particles per cluster, defined as those particles for which $|\psi_6|^2 \geq 0.9$. In Fig. 3 we show contour plots of $-\ln(n/n_1)$ vs. N and N_c , where n is the number of clusters in 6–8 min of video having N and N_c within a given range of values (a similar analysis was used in [39]). We thereby obtain the free energy of clusters, $F_{\text{clu}}/k_B T$. For the 17% sample, the optimal (lowest- F_{clu}) path has N_c growing with N and $F_{\text{clu}} \sim 6k_B T$ when $N = 25$ [Fig. 3(a)]. For the 30% sample, F_{clu} would be $\sim 9k_B T$ if the same trajectory were followed [faint dashed curve of Fig. 3(b)]; instead these clusters first grew, then developed order. This trajectory lowered F_{clu} to $\sim 5.5k_B T$ when $N = 25$.

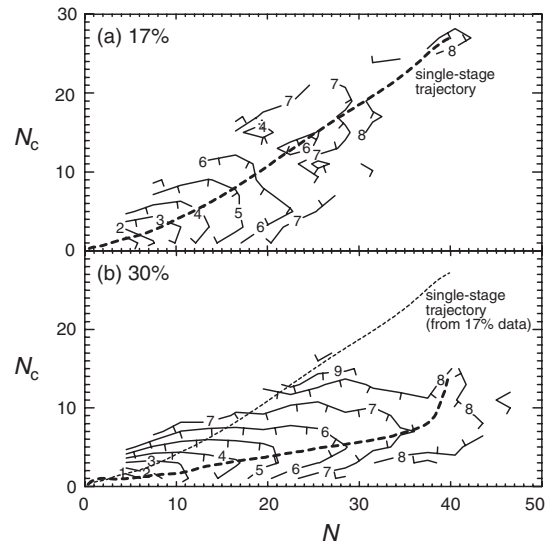


FIG. 3. Contour plots of the cluster free energy $F_{\text{clu}}/k_B T \equiv -\ln(n/n_1)$, where n is number density of clusters with N total particles and N_c crystalline particles. In each case, the value at the origin is zero and the blank regions contain no data. The lowest- F_{clu} trajectory for each plot is shown with the heavy dotted line (drawn freehand). The trajectory for the 17% sample is reproduced on the lower plot for comparison.

Nucleation free-energy barriers calculated from Monte Carlo simulations with short-range attraction in 3D showed similar optimal trajectories [9]. There, a single-step nucleation process was followed above and below the metastable g - l critical temperature, T_c . At T_c , however, the lowest- F_{clu} path corresponded to growth of liquidlike clusters that ordered at a cross-over size of $N \sim 200$. The cross-over size of 30–40 found from Fig. 3(b) (in 2D) is comparable in value, since $200^{2/3} \approx 34$.

The largest cross-over size and enhanced nucleation rates were observed here in samples with $\eta \approx 30\%$, reasonably close to the predicted (metastable) g - l critical $\eta \approx 40\%$ in 2D [34]. Previous studies with short-range depletion attraction in dilute samples (2% in 3D [40], and 16% in 2D [41]) showed nucleation of crystals after a shallow quench and diffusion-limited structures after a deeper quench. These observations are consistent with our results for 17% and 18.5%, suggesting that the classical nucleation generally occurs at concentrations far below the metastable critical concentration (at least for shallow quenches).

In 2D, the optimal short-range packing is the same as the crystal packing. Hence crystallization occurred rapidly once the crystallites were energetically favorable. In 3D, the locally optimal packing is incommensurate with the crystal and crystallization might be further slowed [4,42]; in this case the fluid clusters might grow to even larger size before ordering, or become trapped in a disordered gel [5,40].

Our results show directly and with single-particle resolution that nucleation can proceed by multiple distinct steps following a quench. (A similar process also occurs in sublimation [24]). With $\eta = 30\%$, this pathway lowered the measured free-energy barrier by at least $3.5k_B T$ relative to the classical nucleation path, which was followed at lower η . Measured line tensions and chemical potentials show how the metastable liquid lowered the energy barrier and enhanced the crystal nucleation rate inside the metastable g - l coexistence region. A similar mechanism is predicted among atoms and molecules with long-range interactions below the triple point [7,16,27,43–45].

We thank Donald Blair, Alex Levine, Robert Guyer, and Liquan Pei for valuable discussions. Funding for this work came from the National Science Foundation (DMR-0605839) and the Research Corporation through a Research Innovation grant.

*Present address: Department of Physics, Cornell University, NY 14853, USA.

- [1] A. Laaksonen, V. Talanquer, and D. W. Oxtoby, *Annu. Rev. Phys. Chem.* **46**, 489 (1995).
- [2] V. J. Anderson and H. N. W. Lekkerkerker, *Nature (London)* **416**, 811 (2002).
- [3] R. P. Sear, *J. Phys. Condens. Matter* **19**, 033101 (2007).
- [4] F. Trudu, D. Donadio, and M. Parrinello, *Phys. Rev. Lett.* **97**, 105701 (2006).
- [5] F. Renth, W. C. K. Poon, and R. M. L. Evans, *Phys. Rev. E* **64**, 031402 (2001).
- [6] S. Y. Chung *et al.*, *Nature Phys.* **5**, 68 (2009).
- [7] J. W. Cahn, *J. Am. Ceram. Soc.* **52**, 118 (1969).
- [8] P. R. ten Wolde and D. Frenkel, *Chem. Phys.* **1**, 2191 (1999).
- [9] P. R. ten Wolde and D. Frenkel, *Science* **277**, 1975 (1997).
- [10] K. G. Soga, J. R. Melrose, and R. C. Ball, *J. Chem. Phys.* **110**, 2280 (1999).
- [11] A. Lomakin, N. Asherie, and G. B. Benedek, *Proc. Natl. Acad. Sci. U.S.A.* **100**, 10254 (2003).
- [12] V. Talanquer and D. W. Oxtoby, *J. Chem. Phys.* **109**, 223 (1998).
- [13] C. Haas and J. Drenth, *J. Phys. Chem. B* **104**, 368 (2000).
- [14] A. Shiryayev and J. D. Gunton, *J. Chem. Phys.* **120**, 8318 (2004).
- [15] D. Kashchiev, P. G. Vekilov, and A. B. Kolomeisky, *J. Chem. Phys.* **122**, 244706 (2005).
- [16] J. F. Lutsko and G. Nicolis, *Phys. Rev. Lett.* **96**, 046102 (2006).
- [17] D. Vivares, E. W. Kaler, and A. M. Lenhoff, *Acta Crystallogr. Sect. D* **61**, 819 (2005).
- [18] O. Galkin *et al.*, *Biophys. J.* **93**, 902 (2007).
- [19] O. Galkin and P. G. Vekilov, *Proc. Natl. Acad. Sci. U.S.A.* **97**, 6277 (2000).
- [20] C. A. Murray and D. H. van Winkle, *Phys. Rev. Lett.* **58**, 1200 (1987).
- [21] E. K. Hobbie, *Phys. Rev. Lett.* **81**, 3996 (1998).
- [22] K. Zahn, R. Lenke, and G. Maret, *Phys. Rev. Lett.* **82**, 2721 (1999).
- [23] A. M. Alsayed *et al.*, *Science* **309**, 1207 (2005).
- [24] J. R. Savage *et al.*, *Science* **314**, 795 (2006).
- [25] Y. Han *et al.*, *Phys. Rev. E* **77**, 041406 (2008).
- [26] U. Gasser *et al.*, *Science* **292**, 258 (2001).
- [27] T. H. Zhang and X. Y. Liu, *J. Am. Chem. Soc.* **129**, 13520 (2007).
- [28] L. J. Chen *et al.*, *Colloids Surf.* **135**, 175 (1998).
- [29] T. Kato and T. Seimiya, *J. Phys. Chem.* **90**, 3159 (1986).
- [30] J. C. Crocker and D. G. Grier, *J. Colloid Interface Sci.* **179**, 298 (1996).
- [31] See EPAPS Document No. E-PRLTAO-102-017922 for supplementary figures. For more information on EPAPS, see <http://www.aip.org/pubservs/epaps.html>.
- [32] C. F. Tejero *et al.*, *Phys. Rev. Lett.* **73**, 752 (1994).
- [33] M. Dijkstra, *Phys. Rev. E* **66**, 021402 (2002).
- [34] M. G. Noro and D. Frenkel, *J. Chem. Phys.* **114**, 2477 (2001).
- [35] G. Foffi *et al.*, *Phys. Rev. E* **65**, 031407 (2002).
- [36] J. F. Lutsko and G. Nicolis, *J. Chem. Phys.* **122**, 244907 (2005).
- [37] D. Frenkel, *Science* **314**, 768 (2006).
- [38] R. P. Sear, *Phys. Rev. E* **59**, 6838 (1999).
- [39] D. Moroni, P. R. ten Wolde, and P. G. Bolhuis, *Phys. Rev. Lett.* **94**, 235703 (2005).
- [40] E. H. A. de Hoog *et al.*, *Phys. Rev. E* **64**, 021407 (2001).
- [41] J. J. Cerda *et al.*, *Phys. Rev. E* **70**, 011405 (2004).
- [42] L. F. Filobelo, O. Galkin, and P. G. Vekilov, *J. Chem. Phys.* **123**, 014904 (2005).
- [43] X. B. Chen *et al.*, *J. Am. Chem. Soc.* **127**, 4372 (2005).
- [44] B. Chen *et al.*, *J. Phys. Chem. B* **112**, 4067 (2008).
- [45] J. A. van Meel *et al.*, *J. Chem. Phys.* **129**, 204505 (2008).